Embedded bioprinting enables precise fabrication of cultured meat with authentic structural properties

Dongwei Wu, Shumin Pang, Sabrina Bäther, Lisa Woelken, Mariia Abyzova, Jordi Morales-Dalmau, Astrid Haibel, Yunpeng Jia, Johanna Berg, Benedikt B Kaufer, et al.

Food Hydrocolloids 171 (2026) 111795

Contents lists available at ScienceDirect

Food Hydrocolloids

journal homepage: www.elsevier.com/locate/foodhyd

Embedded bioprinting enables precise fabrication of cultured meat with authentic structural properties

Dongwei Wu [a], Shumin Pang [a,b], Sabrina Bäther [c,d], Lisa Woelken [e], Mariia Abyzova [f,g], Jordi Morales-Dalmau [g], Astrid Haibel [h], Yunpeng Jia [i], Johanna Berg [a], Benedikt B. Kaufer [j], Caroline Denesvre [k], Anja Maria Wagemans [c,d], Cornelia Rauh [e], Jens Kurreck [a,*]

[a] Technische Universität Berlin, Chair of Applied Biochemistry, Straße des 17. Juni 135, 10623, Berlin, Germany
[b] Technische Universität Berlin, Chair of Advanced Ceramic Materials, Straße des 17. Juni 135, 10623, Berlin, Germany
[c] Technische Universität Berlin, Department of Food Biosciences, Straße des 17. Juni 135, 10623, Berlin, Germany
[d] Technische Universität Dresden, Chair of Food Engineering, Bergstraße 120, 01069, Dresden, Germany
[e] Technische Universität Berlin, Department of Food Biotechnology and Food Process Engineering, Straße des 17. Juni 135, 10623, Berlin, Germany
[f] Leibniz University of Hanover, Institute of Technical Chemistry, Hanover, Germany
[g] Cultimate Foods GmbH, Berlin/Hannover, Germany
[h] Berliner Hochschule für Technik, Fachbereich II Mathematics-Physics-Chemistry, Luxemburger Str. 10, 13353, Berlin, Germany
[i] Birmingham City University, Department of Life Science, Faculty of Health, Education and Life Sciences, Birmingham, UK
[j] Freie Universität Berlin, Institute of Virology, Berlin, Germany
[k] INRAE, Université de Tours, ISP, Equipe Biologie des Virus Aviaires, F-37380, Nouzilly, France

ARTICLE INFO

Keywords:
Bioprinted meat
Muscle and fat structures
Alginate hydrogel
Rheology
Bioink

ABSTRACT

Cultured meat has emerged as a promising alternative to conventional meat, offering potential solutions to environmental, ethical, and health-related concerns. However, current technologies often yield unstructured products like minced meat, falling short of replicating the complex architecture and marbling of natural cuts, which are the key factors for consumer acceptance. This study utilizes a hybrid fabrication approach combining casting and embedded 3D bioprinting to produce cultured meat with complex structured architectures, leading to improvements in both print quality and efficiency. Muscle tissue, the main structural component, was first cast using a hydrogel-cell mixture, followed by precise deposition of adipocytes to create intricate fat structures. We demonstrate that this method incorporated with alginate hydrogel was compatible with chicken and pork cell types. It enabled the production of artificial cultured meat resembling pork, beef, and fish. To replicate the natural structure of meat, we used micro-computed tomography (μCT) to capture the fine architecture of a pork steak. A computational algorithm then segmented muscle and fat regions for obtaining their 3D models, allowing the fabrication of a negative mold for casting muscle portion and the acquisition of deposition paths for embedded bioprinting fat component. Oil-emulsion food dyes were employed to replicate the natural coloration of meat. The resulting cultured meat closely mimicked the structural complexity of its natural counterpart. By recreating the appearance of conventional meat, this approach has the potential to enhance consumer acceptance and facilitate the transition to more sustainable and ethical meat alternatives.

1. Introduction

In recent years, the global food landscape has faced growing challenges, including climate change, food security concerns, and the ethical implications of traditional livestock farming (Godde et al., 2021). With the world's population projected to reach nearly 10 billion by 2050, the demand for meat is expected to rise dramatically (Meyers & Kalaitzandonakes, 2015; Wanapat et al., 2024). However, conventional meat production is resource-intensive and significantly contributes to greenhouse gas emissions, deforestation, and biodiversity loss (M. Lee et al., 2024). In response, cultured meat, also known as lab-grown or cell-based meat, has emerged as a promising sustainable and ethical

* Corresponding author.
E-mail address: jens.kurreck@tu-berlin.de (J. Kurreck).

https://doi.org/10.1016/j.foodhyd.2025.111795
Received 28 April 2025; Received in revised form 18 July 2025; Accepted 21 July 2025
Available online 25 July 2025

alternative to conventional meat production (K. Handral, Shi, Weng, & and Choudhury, 2022; Martins et al., 2024).

Cultured meat is produced by cultivating animal cells or cell-laden biomaterials in a controlled environment, eliminating the need for raising and slaughtering animals. This technology offers several advantages, including reducing antibiotic and hormone use, minimizing contamination risks from foodborne pathogens, and potentially enhancing nutritional value (Woelken et al., 2024). Separately, cultured meat addresses sustainability and ethical considerations associated with conventional livestock farming, and presents an opportunity to develop a healthier and more efficient method of meat production (Klatt et al., 2024; Post et al., 2020).

Despite its potential, several challenges hinder the widespread commercialization and adoption of cultured meat. One of the key obstacles is the technological complexity of replicating the intricate structure and texture of traditional meat. Natural meat consists of muscle fibers, fat cells, and connective tissues, each contributing to its structure, texture, flavor, and mouthfeel – critical factors for consumer acceptance (Roy & Bruce, 2024). Current cultured meat products often struggle to achieve the same sensory attributes, making structure and texture engineering a key focus of research.

To address this challenge, 3D bioprinting has emerged as a promising technology for fabricating structured meat products (Ozbolat et al., 2016; Santoni et al., 2022). This approach enables the precise deposition of bioinks – comprising living cells, biomaterials, and other essential components – in a layer-by-layer fashion to create complex tissue constructs (Berg & Kurreck, 2021). By engineering muscle and fat tissues in controlled configurations, 3D bioprinting offers the potential to closely mimic the natural structure and composition of conventional meat. Additionally, by modifying bioink composition and printing parameters, it is possible to fine-tune the flavor, nutritional profile, texture and structure of cultured meat.

In recent years, both academic researchers and industry pioneers have explored 3D bioprinting for cultured meat production. Initial studies primarily employed extrusion-based bioprinting, fabricating thin layers or small constructs, successfully demonstrating the feasibility of this approach (Albrecht et al., 2024; Guo et al., 2024; Gurel et al., 2024). However, these early models lacked the structural complexity and scale required to replicate real meat. More recently, Kang et al. (Kang et al., 2021) engineered meat-like tissues by integrating three types of bovine cell fibers, including muscle, fat, and vascular tissues, via bioprinting, advancing the field toward more realistic tissue-like structure. On the industrial front, companies such as Revo Foods (Austria) and Redefine Meat (Israel) have developed bioprinted meat products using multiple printheads to extrude muscle and fat components in filament-wise and layer-wise configurations. While these techniques show promise, they face limitations, including low efficiency and the need to balance printing speed and resolution, posing challenges for scalability. Consequently, achieving high-fidelity, scalable 3D bioprinting of cultured meat remains an ongoing challenge in both research and commercial settings.

To overcome the limitations of traditional extrusion-based bioprinting, embedded bioprinting has emerged as an innovative alternative. This technique involves extruding bioinks within a supportive hydrogel matrix, allowing for the fabrication of intricate, multi-component structures with enhanced structural integrity (Zeng et al., 2022) in an efficient manner. The supporting hydrogel stabilizes the bioinks, opening up new possibilities for creating complex architectures that closely resemble natural meat structures.

Embedded bioprinting also allows for fine-tuning mechanical properties by incorporating various biomaterials, theoretically achieving textures and mouthfeel similar to conventional meat (Marques et al., 2025; Schätzlein & Blaeser, 2022). A critical aspect of this approach is the development of optimized bioinks that support cell viability, proliferation, and functionality, while maintaining printability and structural fidelity. Furthermore, technological developments are required to achieve precise control over meat structure and ensure high-resolution replication of natural meat structures.

To address these challenges, this study aims to develop an efficient and scalable procedure for bioprinting cultured meat using embedded bioprinting techniques. We introduce a hybrid approach, integrating casting methods with bioprinting to fabricate structured meat products. In the first step, muscle tissue was formed by casting muscle component in a multi-well plate in the initial experiments or a custom 3D-printed steak-shaped mold in later stages as a support bath. Subsequently, fat tissue was then precisely distributed in desired structures within the muscle matrix using needle extrusion from a pneumatic cartridge. We also demonstrate that this approach can replicate the structure of a natural pork steak captured through μCT imaging. By combining casting and embedded bioprinting, this approach enables the fabrication of cultured meat with diverse structures, closely mimicking traditional meat products while ensuring efficiency and scalability.

2. Experimental section

2.1. Preparation of alginate solutions

Sodium alginate (alginic acid sodium salt, high viscosity, ThermoFisher (Kandel) GmbH, Kandel, Germany) was dissolved in Hank's Balanced Salt Solution (HBSS, Biowest, Nuaillé, France) under agitation for 4 h at room temperature to prepare homogeneous solutions at 1 %, 2 %, and 3 % (w/v) concentrations. The solutions were then transferred into 50 mL syringes (BD Plastipak, New Jersey, USA), with plungers removed and outlets sealed using Luer blockers. To eliminate air bubbles, the loaded syringes were centrifuged at 300 g for 5 min. The plunger was then carefully reinserted with the aid of a 20G needle to expel any remaining air between the rubber stopper and the alginate solution. Finally, the prepared syringes were stored at 4 °C overnight for aging before use or measurement.

2.2. Rheological measurement

Rheological properties of the prepared alginate solutions were analyzed using a rotational rheometer (Anton Paar, Physics MCR 301, Graz, Austria) with a 25 mm parallel steel plate setup. The test gap was set to 1 mm, and measurements were conducted at 25 °C. An amplitude sweep with a shear strain range of 0.01 %–300 % at 1 Hz was performed to determine the linear viscoelastic region (LVR) and assess the mechanical properties of the samples. To evaluate shear-thinning behavior, a shear rate sweep was conducted within a range of 0.01–300 s^{-1}. Additionally, an oscillatory thixotropy test was applied to assess the suitability of the samples for bioprinting by subjecting them to alternating shear amplitudes: 0.01 % (30 s) – 200 % (30 s) – 0.01 % (180 s). These phases were designed to simulate different stages of the bioprinting process: before extrusion and nozzle movement inside the support bath, during extrusion or nozzle travel, and after extrusion or nozzle travel, respectively. A frequency sweep (0.1 Hz–100 Hz) at 1 % oscillatory shear strain within the LVR was also performed to characterize the viscoelastic response of the samples.

2.3. Cell isolation and culture

Two human embryonic kidney (HEK) cell lines, red fluorescent protein (RFP) labelled HEK293 (HEK293-RFP) and green fluorescent protein (GFP) labelled HEK293 (HEK293-GFP) (GenTarget Inc., San Diego, CA, USA) were employed in this study to indicate different components in the printing structures. They were cultured in Dulbecco's Modified Eagle Medium (DMEM, Biowest) supplemented with 10 % fetal bovine serum (FBS, c.c.pro, Oberdorla, Germany), 4.5 mg/mL glucose (Sigma, Massachusetts, USA), 2 mM L-glutamine (Biowest), 1 × non-essential amino acids (NEAA, Biowest), and 1 × penicillin-streptomycin (Biowest).

The chicken cell line ESCDL-1 (Embryonic Stem Cell Derived Line 1), derived from chicken embryonic stem cells as previously reported (J.-F. Vautherot, Jean, Fragnet-Trapp, Remy, et al., 2017), was propagated in DMEM-F12 (Biowest) supplemented with 10 % FBS and 2 mM L-glutamine. Cells were passaged twice weekly at a 1:3 ratio.

Primary isolation of porcine adipose-derived mesenchymal stem cells (pAD-MSCs) was performed following the protocol by Williams et al. (Williams et al., 2008), with minor modifications. Adipose tissue was collected from a healthy 6-month-old pig at a private slaughterhouse within a 1-h travel radius of the laboratory in Hanover, Germany. In a biosafety cabinet, the tissue was minced into ~1 mm^3 pieces and incubated with a 1 % collagenase I and 1 % dispase II solution in HBSS. Following enzymatic digestion, an equal volume of DMEM/F12 medium with 10 % FBS and 1 % penicillin-streptomycin was added. The mixture was centrifuged at 300 g for 5 min, and the resulting pellet was resuspended, filtered through a 40 μm cell strainer (Sarstedt, Nuembrecht, Germany), and seeded into T75 flasks (Sarstedt). Upon reaching 80–90 % confluency, cells were detached using TrypLE (Thermo Fisher Scientific), counted, and either cryopreserved or further cultured in T175 flasks. Cells were maintained in DMEM/F12 medium supplemented with 10 % FBS, 2 mM L-glutamine, 1 % penicillin-streptomycin, and 2 ng/mL porcine FGF-2 growth factor (pFGF, Faba.Bio, Innocent Meat, Papendorf, Germany).

Porcine fibroblasts were obtained using selection method based on the isolated pAD-MSCs. Specifically, the pAD-MSCs were incubated in T75 flasks overnight at 39 °C and 5 % CO_2. The following day, the culture medium was replaced, and single spindle-shaped cells adhering to the plastic surface were observed. After three days, a colony of cells had formed. At passage 4, the cells showed no differentiation when induced toward adipogenic, osteogenic, or chondrogenic lineages, leading to their classification as fibroblasts. Flow cytometry analysis confirmed that the cells were negative for CD44, CD45, and CD90, further supporting their fibroblast identity.

Porcine adipocytes were derived from pAD-MSCs differentiation. Briefly, adipogenic differentiation of freshly isolated pAD-MSCs was induced in DMEM/F12 supplemented with 2 mM L-glutamine, 1 % penicillin-streptomycin, 50 mg/L ascorbic acid-2-phosphate trisodium salt (MedChemExpress, Monmouth Junction, NJ, USA), 10 μg/mL insulin (Merck, Darmstadt, Germany), 2 μM rosiglitazone (Selleck Biotechnology, Cologne, Germany), 1 μM dexamethasone (Thermo Fisher Scientific), and 0.5 mM 3-isobutyl-1-methylxanthine (Merck). As a serum substitute, 1 % NouSerum (NOUBIO, Los Angeles, CA, USA) was used. After a 3-day induction phase, cells underwent an 18-day lipid accumulation phase, during which 3-isobutyl-1-methylxanthine was excluded (lipid accumulation medium). Media was replaced every three days.

If not otherwise stated, all cells were cultured in a humidified incubator at 37 °C with 5 % CO_2, with media refreshed every 2–3 days.

2.4. Cell viability evaluation

To evaluate biological properties of the alginate matrix, three different animal cells types, ESCDL-1 from chicken, fibroblasts and adipocytes from pork, were respectively blended with alginate hydrogel to achieve a bioink containing 2 % alginate and 5 × 10^6/mL cells. Thin round disc models with thickness of 0.4 mm and diameter of 8 mm were bioprinted in a 48-well plate using the cell-laden bioinks on a 3D bioprinter (BioX6, Cellink, Gothenburg, Sweden) equipped with a pneumatic cartridge (Cellink) and a 22G needle (Cellink). Subsequently, 300 μL of the relevant complete medium supplemented with 25 mM Calcium chloride ($CaCl_2$) was added into each well to cover the model before transferring the well plate into the incubator. At predetermined time points, cell viability was assessed via the XTT assay (Alfa Aesar, Ward Hill, MA, USA) based on metabolic conversion of tetrazolium salt referring to previous study (Wu et al., 2022). The XTT working solution was prepared by mixing 1 mg/mL XTT solution in phenol red-free RPMI 1640 medium (Biowest) with 3.83 mg/mL phenazine methosulfate (AppliChem, Darmstadt, Germany) in phosphate-buffered saline (PBS) at a 500:1 ratio. A total of 150 μL of this solution was added per well in a 48-well plate and incubated at 37 °C with 5 % CO_2 for 4 h. Absorbance was measured at 450 nm (reference: 620 nm) using a microplate reader (Sunrise, Tecan, Männedorf, Switzerland). Constructs without cells served as background controls, and relative viability was normalized to day 1 measurements.

Live/Dead assay (Invitrogen, Thermo Fisher Scientific) was performed to assess cell viability and distribution within bioprinted constructs. After washing samples with PBS, constructs were incubated with a staining solution containing 2 μM calcein AM and 2 μM ethidium homodimer-1 in phenol red-free RPMI 1640 medium for 30 min, followed by fluorescence microscopy imaging (Observer Z1, Zeiss, Jena, Germany).

Confocal microscopy was performed on bioprinted samples containing porcine fibroblasts after 1 and 7 days of culture. A region of 900 × 850 × 100 μm^3 (L × W × H) was scanned using fluorescence microscope (Observer Z1, Zeiss) coupled with a laser scanning confocal system (RCM, Confocal NL, Amsterdam, Netherlands). The resulting image stacks were processed and reconstructed using ImageJ software (National Institutes of Health, MD, USA).

2.5. Bodipy staining

Visualization of lipids was achieved by Bodipy staining. To this end, the bioprinted constructs were collected at predetermined time points and washed three times with HBSS. Subsequently, the samples were fixed with 4 % formaldehyde (Carl Roth, Karlsruhe, Germany) in HBSS supplemented with 25 mM $CaCl_2$ for 30 min and washed another three times before proceeding to direct staining or storage at 4 °C. For lipid staining, a stock solution of BODIPY493/503 (Fisher Scientific) was prepared at a concentration of 5 mM in dimethyl sulfoxide (DMSO, Sigma). A working solution for staining was then prepared by diluting the stock solution 2500 times in HBSS containing 1 μg/mL Hoechst 33342 (Fisher Scientific) for nuclear staining. Staining was conducted in a multi-well plate at room temperature for 2 h. Following staining, the samples were washed three times with HBSS and imaged using fluorescence microscopy. Lipids appeared green, while cell nuclei were visualized in blue.

2.6. Embedded bioprinting

The cell-laden bioink was prepared by mixing 3 % alginate and suspension of chicken mesenchymal cells (ESCDL-1), porcine fibroblasts, or porcine adipocytes with syringe couple method in a volume ratio of 2:1. The final bioink contained 2 % alginate and 5 × 10^6/mL cells. For embedded bioprinting, 2 mL of the bioink containing porcine fibroblasts was cast into each well of a 12-well plate, representing the muscle component of the meat. The casted plate was incubated until it was transferred to the print bed of the BioX6 3D bioprinter just before the printing process. The fat component containing porcine adipocytes was loaded into a 3 mL pneumatic cartridge and mounted onto the printhead of the bioprinter. During printing, both the print bed and printhead were maintained at 37 °C.

2.7. Bioprinting of pork steak sample with natural structure

To illustrate the comprehensive process of generating the pork steak construct, we present detailed fabrication schematics (Fig. 5a and Supplementary Fig. 1), highlighting the systematic approach used to accurately mimic the natural structure of pork steak. The process began with the digital modeling of a real pork steak, capturing the complex spatial organization of muscle and fat tissues. Micro-computed tomography (μCT) was used to obtain a series of original 2D slices, which were then processed with ImageJ program to reduce image noise and a custom

Python script (seeing supplementary materials) to correct non-uniform axial exposure. This refinement enabled precise differentiation between muscle and fat tissues, even when density differences were minimal. The corrected images were then spatially stacked into 3D models, distinguishing muscle and adipose tissues.

Next, the muscle model was digitally inverted to create a negative mold, which was fabricated using fused deposition modeling (FDM) with a Bambu Lab X1C 3D printer (Bambu Lab, Shenzhen, China) and polylactic acid (PLA) filament (DAS FILAMENT, Emskirchen, Germany). The FDM-printed negative mold enabled maintaining the desired shape of the muscle component during the casting process. It also provided mechanical support, ensuring structural stability and fidelity during subsequent bioprinting steps. Within the mold, the muscle bioink, comprising alginate hydrogel mixed with a rust oil-based dye (Rust OIL BLEND, Colour Mill, Happy Sprinkles, Hamburg, Germany) and porcine fibroblasts to simulate muscle tissue, was carefully casted. This casted muscle bioink formed a stable support bath, allowing embedded bioprinting to proceed. As an example of enhancing nutritional value, 5 % pea protein (ProFam Pea Protein 580, lot #E2028107A1, kindly provided by ADM Germany GmbH (Hamburg, Germany)) was incorporated in the muscle bioink additionally. The stock suspensions of pea protein were prepared by dispersing the protein powder in distilled water, followed by stirring for 2 h. The suspension was then homogenized at 17,500 rpm for 90 s using an Ultra-Turrax® homogenizer (IKA-Werke, Staufen, Germany). Subsequently, the suspension was sterilized by autoclaving at 121 °C for 15 min. After autoclaving, the suspension was thoroughly mixed by shaking, cooled in an ice bath for 10 min, and stored at 4 °C overnight.

The fat portion of the 3D model was sliced and converted into a printer-compatible G-code file for bioprinting. The fat bioink, containing white oil-based dye (Sugarflair Colours Ltd, Benfleet, UK) and porcine adipocytes to represent adipose tissue, was then precisely extruded and integrated within the muscle bioink following the prepared G-code instructions.

After bioprinting, the entire construct was stabilized through ionic crosslinking by spraying it with a 25 mM $CaCl_2$ solution, which reinforced the hydrogel network and preserved the structure of the bioprinted meat. The spray was applied using a 10 mL syringe fitted with an intranasal mucosal atomization device (MAD Nasal™, Teleflex Medical GmbH, Fellbach, Germany), ensuring an even and efficient crosslinking process.

2.8. Statistics

Experiments were performed in triplicates unless otherwise stated. Data are presented as mean ± standard deviation (SD). Statistical analyses were conducted using Prism 9 software (GraphPad, Boston, MA, USA), employing either Student's t-test or one-way ANOVA method. Statistical significance was defined as follows: *$p < 0.05$, **$p < 0.01$, ***$p < 0.001$, and ****$p < 0.0001$.

3. Results

3.1. Optimization of hydrogel formulation for embedded bioprinting

Embedded printing extrudes materials into a support bath to create complex 3D structures, unlike direct ink writing, which deposits material into the air. The embedded printing technology is particularly advantageous for fabricating multi-component structures, where one component constitutes the bulk while others are strategically deposited within it. This advantage is even more pronounced when producing structures with one major component and additional minor ones (Supplementary Fig. 2). In meat products, muscle typically forms the larger portion, while fat represents a smaller component. Consequently, muscle serves as the primary structure, with fat tissue as the secondary component. In this study, embedded bioprinting was utilized to enhance production efficiency, enabling the creation of meat structures with precisely controlled compositions.

To achieve effective embedded bioprinting, a suitable hydrogel formulation is essential for maintaining the integrity of the dispensed components within the support matrix. Alginate is a widely used polysaccharide that can be crosslinked with calcium or other divalent ions to form a hydrogel (Choi et al., 2022). This ionically crosslinked alginate hydrogel is commonly employed in 3D bioprinting, food science and drug delivery, due to its advantages of renewability, low cost, excellent printability, and good cell compatibility (Tao et al., 2024; D. Wu, Pang, et al., 2024). Therefore, it was selected as the primary component for both support bath and extrusion dispensing in embedded bioprinting in this study.

To determine the optimal alginate concentration for bioprinting, rheological measurements were conducted. An amplitude sweep (0.01 %–300 %) was performed on samples of alginate/HBSS formulas at concentrations of 1 %, 2 %, and 3 %. As shown in Fig. 1a, 1 % alginate exhibited a liquid-like state (storage modulus G' < loss modulus G″), indicating that it flows away too easily and cannot support the structure of the dispensed material, making it unsuitable for bioprinting. In contrast, 2 % and 3 % alginate demonstrated solid-like behavior at lower amplitude ranges (<9.66 % for 2 % alginate and <35 % for 3 % alginate) (Fig. 1a). This solid-like behavior results from the formation of a strong network due to increased chain entanglement and intermolecular interactions in the alginate solution.

At high shear strain, the alginate network was disrupted, causing both 2 % and 3 % alginate samples to transition into a liquid-like state. This test confirms the shear-thinning behavior of the material, further supported by the shear rate sweep results, which show a decrease in viscosity for all three samples as the shear rate increased (Fig. 1b). This shear-thinning property is a crucial characteristic for both the support and dispensed components in embedded bioprinting. On the one hand, the reduced viscosity under shear allows the printing needle to move easily through the support phase with minimal resistance. On the other hand, the extruded material flows smoothly from the nozzle during deposition.

The thixotropic properties of 2 % and 3 % alginate were evaluated using a strain-switching test. As shown in Fig. 1c, both samples (excluding 1 %) transitioned through solid-like, liquid-like, and solid-like states under a low-high-low shear amplitude cycle. Following high shear, both 2 % and 3 % alginate hydrogels regained their solid-like structure as the alginate network began to recover. This recovery indicates that the network breakdown under the applied high shear strain is reversible, which is essential for maintaining structural stability after printing.

Additionally, the frequency sweep test demonstrates that higher alginate concentrations form more stable structures. The storage modulus remained stable at shear frequencies below 39.8 Hz for 2 % alginate and 63.1 Hz for 3 % alginate. In contrast, 1 % alginate showed a significant drop at a much lower frequency (1.58 Hz), indicating that it had a weak network and was not suitable for bioprinting which requires structural integrity.

The alginate formulations were further assessed through embedded bioprinting of a designed zig-zag patterned model (Fig. 1e). The results aligned with the rheological tests, confirming that 1 % alginate was too fluid-like to maintain the printed structure. As expected, 2 % and 3 % alginate hydrogels produced well-defined patterns, making them more suitable for embedded bioprinting.

However, a higher alginate concentration does not necessarily yield better results. Excessive viscosity can hinder the casting of the support component, which, in this case, represents the muscle phase. To evaluate this, we examined the casting behavior of the hydrogels by extruding them into a 6-well plate followed by automated shaking. As shown in Fig. 1f, 2 % alginate exhibited superior casting properties compared to 3 % alginate, which was excessively stable. The 3 % alginate hydrogel maintained its filament-like shape under extrusion and failed to spread

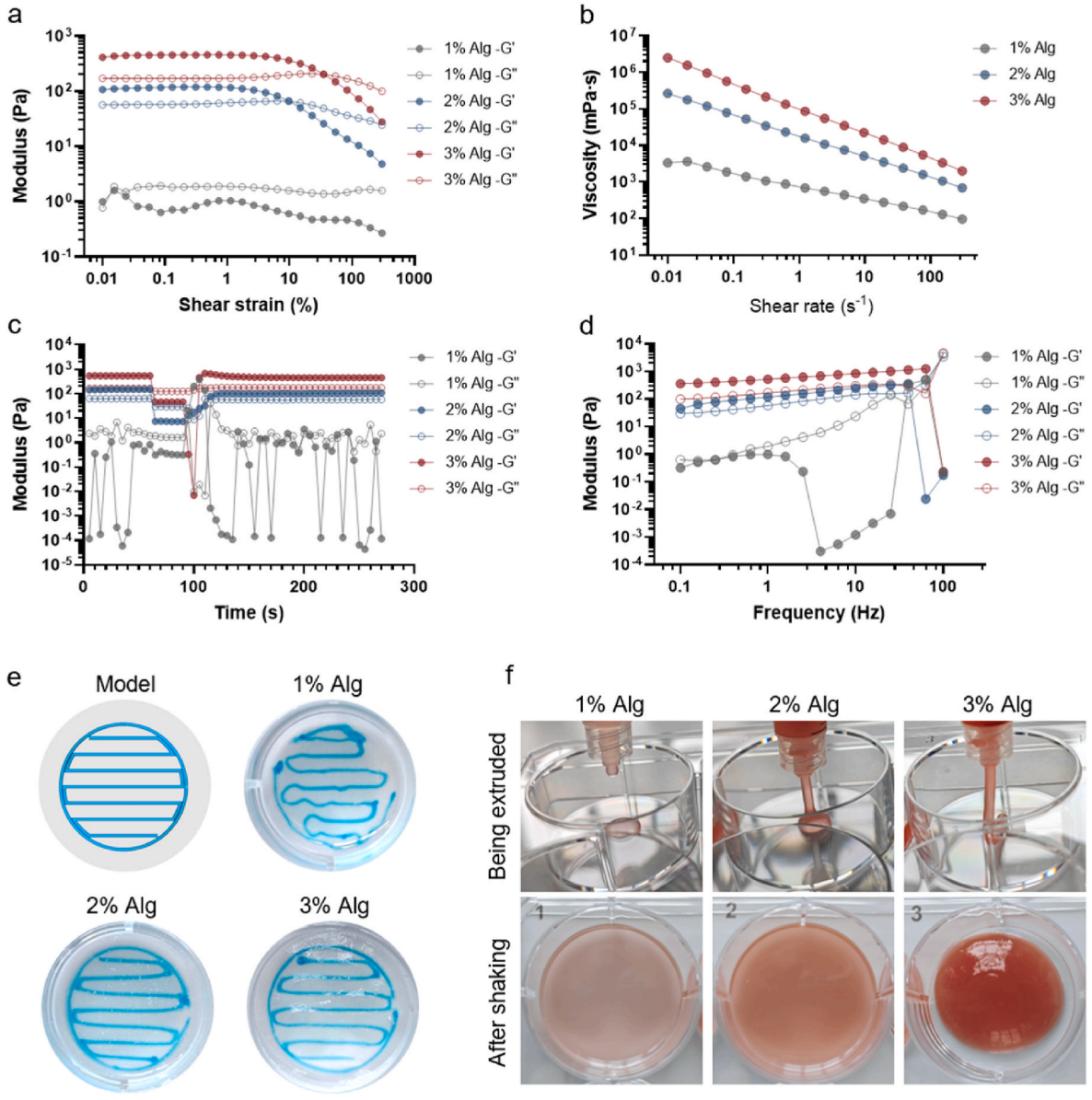

Fig. 1. Optimization of alginate formulation for embedded bioprinting. Rheological properties of alginate (Alg) hydrogels were assessed through (a) amplitude sweep, (b) shear rate sweep, (c) three-step strain-switching test, and (d) shear frequency sweep (G′: storage modulus; G″: loss modulus.). Embedded bioprinting performance (e) and casting behavior (f) were analyzed for the pristine alginate hydrogels at different concentrations.

evenly, even after 30 s of automatic shaking with the Tecan system. In contrast, 2 % alginate successfully formed a well-cast and uniform layer. Therefore, these results confirmed that 2 % alginate is optimal for both casting and extrusion, which are the key processes involved in embedded bioprinting of structured meat models.

3.2. *Biocompatibility of alginate hydrogel incorporating chicken and porcine cells*

After selecting the 2 % alginate hydrogel formulation due to its favorable rheological properties and effective casting behavior, a comprehensive evaluation of cellular compatibility was conducted to confirm its suitability for bioprinting cultured meat constructs. This assessment focused on several cellular systems, including a chicken cell line (ESCDL-1) derived from chicken embryonic stem cells (J. F. Vautherot, Jean, Fragnet-Trapp, Remy, et al., 2017), porcine fibroblasts, and porcine adipocytes, in order to assess the biocompatibility of the hydrogel across a range of cell types relevant to food production applications.

Alginate, a water-soluble polysaccharide, can be crosslinked by multivalent cations to form stable hydrogels. In this study, a bioink consisting of 2 % alginate and 5 × 10^6 animal cells/mL was prepared and bioprinted into disc models on a multi-well plate. Calcium chloride ($CaCl_2$) was then used as the crosslinking agent in the complete medium for cultivation of the printed models. The 2 % alginate solution remained stable across all three tested concentrations of $CaCl_2$ (25, 50, and 100 mM) throughout the culture period (data not shown).

Initial biocompatibility experiments were conducted using chicken ESCDL-1 cells encapsulated in the 2 % alginate hydrogel, with ionic crosslinking performed post-bioprinting using $CaCl_2$. These studies provided key insights into the interactions between the encapsulated cells and the hydrogel matrix. Metabolic activity assays using the XTT method indicated that the 25 mM $CaCl_2$ concentration provided the optimal environment, with significantly higher metabolic activity observed over a 7-day culture period compared to the intermediate (50 mM) and higher (100 mM) concentrations (Fig. 2a). A high concentration of $CaCl_2$ (100 mM) leads to strong gels, potentially resulting in over-

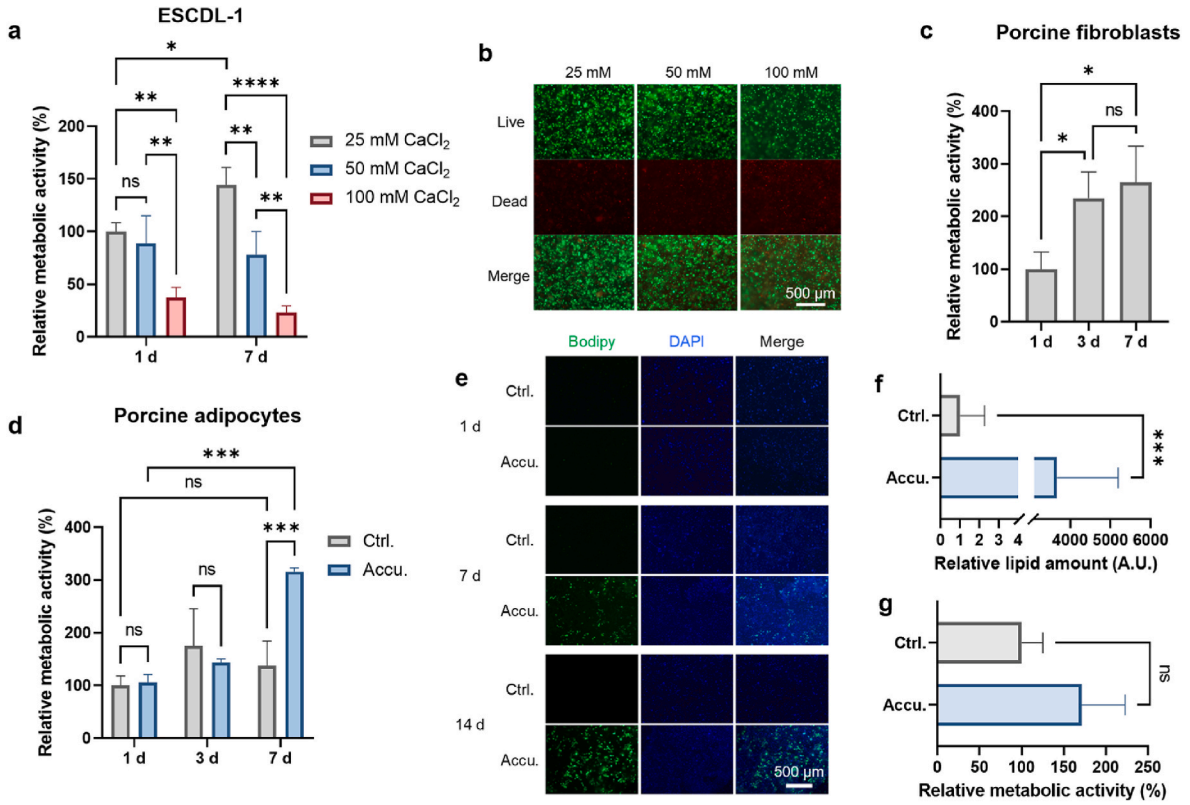

Fig. 2. Biocompatibility evaluation of alginate hydrogel. Chicken ESCDL-1 cells were bioprinted with 2 % alginate hydrogel and cultured in medium supplemented with varying concentrations of $CaCl_2$ as a crosslinking agent. (a) Metabolic activity of ESCDL-1 cells was assessed using the XTT assay. (b) Cell viability of ESCDL-1 was evaluated using a live/dead staining kit. (c) Relative metabolic activity of porcine fibroblasts was measured after bioprinting with the alginate hydrogel, $CaCl_2$ crosslinking and subsequent incubation. (d) Porcine adipocytes were tested for cellular compatibility by assessing metabolic activity post-bioprinting in either complete medium (Ctrl.) or lipid accumulation medium (Accu.). (e) Lipid accumulation in porcine adipocytes was visualized using Bodipy (lipid-specific) and DAPI (nuclear-specific) fluorescence staining. (f) Quantitative analysis of lipid accumulation in porcine adipocytes. (g) Relative metabolic activity of bioprinted porcine adipocytes cultured in either complete medium (Ctrl.) or lipid accumulation medium (Accu.) for 14 days.

association of the alginate chains (Bäther et al., 2024). The significantly reduced cell survival at this concentration indicates that excessive crosslinking density can be detrimental. The results suggest that a lower crosslinking density, achieved with 25 mM $CaCl_2$, offers adequate mechanical stability while maintaining better nutrient diffusion, which is crucial for cell survival and metabolic function. Additionally, live/dead staining of ESCDL-1 cells revealed that as the $CaCl_2$ concentration increased from 25 mM to 100 mM, the number of living cells (green fluorescence) decreased, and the number of dead cells (red fluorescence) increased, further confirming the cytocompatibility of the alginate-based scaffold (Fig. 2b).

To broaden the biocompatibility analysis, porcine fibroblasts were also tested, as they are representative of muscle tissue in engineered pork. Metabolic activity assessments showed a significant increase in fibroblast viability from day 1 to day 7 post-bioprinting, indicating cell recovery, adaptation, and proliferation within the hydrogel (Fig. 2c and Supplementary Fig. 3). These results confirm the compatibility of porcine fibroblasts with the alginate matrix and their ability to survive and proliferate after bioprinting. A similar pattern was observed for porcine adipocytes in both control and adipogenic medium, suggesting that the hydrogel is suitable for adipose tissue engineering (Fig. 2d). Notably, porcine adipocytes were measured with significantly higher cell viability in lipid accumulation medium than those in complete medium after culture for 7 days, which was also confirmed by Live/Dead assay (Supplementary Fig. 4). This can be attributed to the addition of the adipogenic supplements, especially insulin and rosiglitazone. Insulin increases glucose transport and glycolytic enzyme activities (Dimitriadis et al., 2011), while rosiglitazone can improve the function of insulin, reduce metabolic stress and support cellular health (Aydemir et al., 2020; Liu et al., 2009). Therefore, these combined effects enhanced glucose uptake and utilization, and provided a more favorable condition for cell growth and function, which led to improved cell viability.

Lipid accumulation is an important process for cultured meat production, as it contributes to fat content in the final product. To evaluate the functional capacity of the alginate hydrogel for adipocyte maturation, porcine adipocytes were cultured in a lipid accumulation medium. As shown in Fig. 2e and f, the adipocytes cultured in the adipogenic medium exhibited significant lipid accumulation, as evidenced by Bodipy fluorescent staining and quantitatively confirmed through lipid content analysis. Compared to the control group (cultured in standard growth medium without adipogenic supplements), the adipogenic conditions led to a substantial increase in lipid synthesis and storage, over 3500-fold. Additionally, adipogenic supplements were found to enhance cell metabolism and activity (Fig. 2d–g), which may be due to the presence of dexamethasone, rosiglitazone, and insulin ensuring critical signals necessary for their differentiation and metabolic functions (Contador et al., 2015; Mills, 1999). These findings confirm that the alginate hydrogel effectively supports functional adipocyte survival, maturation, and lipid accumulation. Based on these results, the 2 % alginate hydrogel was confirmed for the fabrication of cultured meat constructs.

3.3. *Validation of alginate hydrogel for embedded bioprinting*

To produce cultured meat structures with high stability and quality, achieving structural precision and reproducibility in the embedded

bioprinting process is essential. Embedded bioprinting generally involves the deposition of extruded material filaments from a nozzle into a support bath. In this study, we tested the printing of filament structures using the selected 2 % alginate hydrogel. To validate the accuracy of the hydrogel formulation and printing process, filament structures of various lengths (1 mm, 3 mm, 5 mm, and 10 mm) and quantities were designed and printed within the alginate support bath (Fig. 3a). The results demonstrated that the printed filaments closely matched their computational designs, with particularly high precision for longer filament lengths (≥3 mm). The steady flow of material from the nozzle during the printing of longer filaments was facilitated by the favorable rheological properties of the alginate bioink (Fig. 1a–d). In contrast, printing shorter filaments posed challenges due to the need for rapid and frequent adjustments to material dispensing and nozzle movement.

To further assess spatial distribution and cellular compatibility, 3-mm filaments containing fluorescently labelled HEK293 cells (HEK293-RFP in red and HEK293-GFP in green) were sectioned and analyzed using the ChemiDoc Imaging System (Fig. 3b). Fluorescent HEK293 cells were selected for this proof-of-concept study due to their robust growth characteristics, and well-established use in imaging-based assays. Cell distribution can be assessed based on the fluorescence emitted by RFP or GFP in the corresponding cell type. Fluorescent imaging confirmed that both cell types were correctly deposited and uniformly distributed in their designated regions within the printed construct. The clear merging of red and green fluorescence confirmed that embedded bioprinting effectively supports the deposition and spatial distribution of multiple cell types within a single printed structure. This result underscores the potential of embedded bioprinting for creating complex meat tissues with spatially organized muscle and adipose cells.

To evaluate the method's performance under increased complexity, designs with varying filament densities (5 %, 10 %, 20 %, and 30 % volume ratio of deposited filaments) and randomly arranged filaments were prepared and printed (Fig. 3c). The printed structures were well-replicated, demonstrating the excellent printing performance and accuracy of the system. This capability is essential for producing complex patterns with spatially distributed components, similar to the structure of cultured meat. Quantitative reproducibility was assessed by measuring grayscale intensity profiles across the printed constructs in three independent trials (Fig. 3d and Supplementary Fig. 5). The data showed highly consistent profiles across replicates, confirming the reproducibility of the printing process and highlighting the optimal conditions for fabricating reliable bioprinted structures.

These findings demonstrate that the embedded bioprinting process, using the established configurations, can generate highly reproducible, precise, and robust alginate hydrogel structures. The results validate both the bioprinting procedure and the performance of the selected 2 % alginate formulation. This formulation successfully supports the survival and integration of multiple cell types critical for muscle and adipose tissue development, making it a promising method for efficiently producing cultured meat products with complex, customizable internal structures.

3.4. Embedded bioprinting of artificial meat structures

Building upon the validation of alginate-based embedded bioprinting, we aimed to replicate natural meat structures by precisely controlling the spatial distribution of muscle and adipose components. Real meat products typically consist of a predominant muscular portion interspersed with minor fat deposits. To mimic this architecture, we employed a bioprinting system using two distinct cell populations -

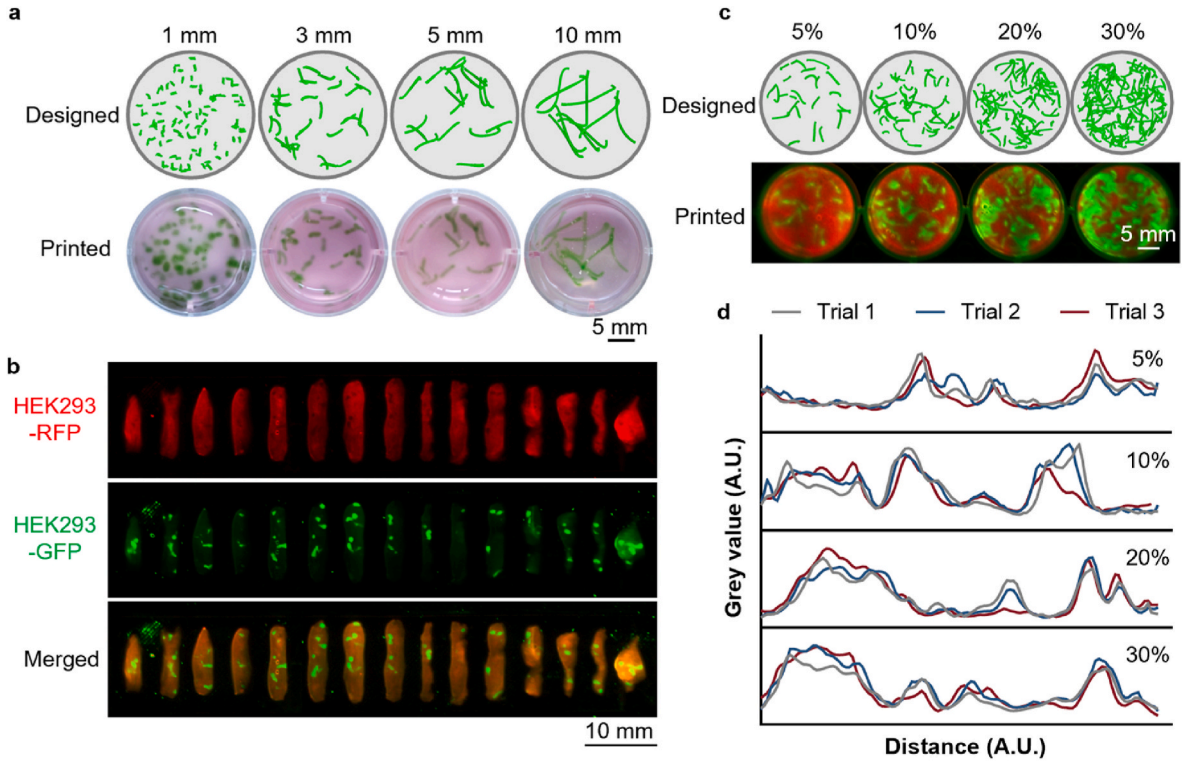

Fig. 3. Validation and reproducibility of embedded bioprinting with alginate hydrogel. (a) Filament structures of varying lengths were deposited in a support bath using embedded bioprinting. The upper panel shows the designed models, while the lower panel displays optical images of the fabricated objects after the bioprinting process. The green color originates from green food dye. (b) A 3-mm filament sample was sectioned into thin slices and analyzed using the ChemiDoc Imaging System. The red fluorescence signal was emitted by RFP in HEK293-RFP cells, and the green fluorescence signal was from GFP in HEK293-GFP cells. (c) Models with filaments of random lengths and varying quantities were also printed. The upper panel shows the model design, while the lower panel presents fluorescence images of the printed structures. (d) Reproducibility of the printing process was tested by repeating the bioprinting of structures with varying filament amounts three times. The gray value of the HEK293-GFP fluorescence channel was measured at the middle area of each sample in all three repetitions.

HEK293-RFP cells (red fluorescence) representing muscle tissue and HEK293-GFP cells (green fluorescence) representing adipose tissue. The optimized 2 % alginate hydrogel, previously validated for its rheological properties, cell viability, and stability, served as both the support and extruding bioink material.

To demonstrate the capability of embedded bioprinting in fabricating structured meat architectures, we designed and printed four different models resembling various meat features: pork, beef, fish, and a whole steak. These designs were developed based on qualitative visual observations of real meat cuts, focusing on overall structural patterns with the aim of replicating visually recognizable major features, serving as representative models for future refinement. The constructs with adipose structures printed within the muscle cell support bath closely replicated their computational designs, successfully recreating the intended spatial arrangement of muscle and fat components (Fig. 4, left panel). Optical images confirmed the precise embedding of adipose structures within the muscular matrix, with muscle tissue represented in red and fat tissue in green.

Fluorescence imaging provided further insights into the spatial fidelity of the printed structures. As shown in Fig. 4 (middle panel), the post-printing distribution of HEK293-RFP and HEK293-GFP cells closely mirrored the original computational models, with minimal diffusion or displacement of components. This confirmed the robustness of the embedded bioprinting technique in maintaining structural integrity.

At higher magnifications, fluorescence microscopy revealed well-defined boundaries between muscle and adipose tissues, with clear separation of red and green fluorescent regions at the microscale (Fig. 4, right panel). This level of precision is crucial for mimicking the natural microstructure of meat, enhancing its textural realism. Notably, the exceptional flexibility of 3D bioprinting allows for easy customization of fat content within printed meat constructs, catering to specific dietary preferences or culinary applications (Supplementary Fig. 6). Additionally, the structure and consequently the texture and mouthfeel of meat products can be significantly influenced by slicing orientation, which was successfully controlled by adjusting the bioprinting model and parameters (Supplementary Fig. 7). This adaptability can be used to produce cultured meat tailored for different consumer preferences and cuisines.

The successful fabrication of a steak-shaped construct further demonstrated the applicability of embedded bioprinting for realistic meat production (Fig. 4d). The steak-like structure accurately integrated minor fat components within the dominant muscle matrix, closely resembling the natural composition of conventional meat. Optical and fluorescence imaging confirmed the homogeneity of component distribution and the high degree of structural control achievable with this bioprinting approach.

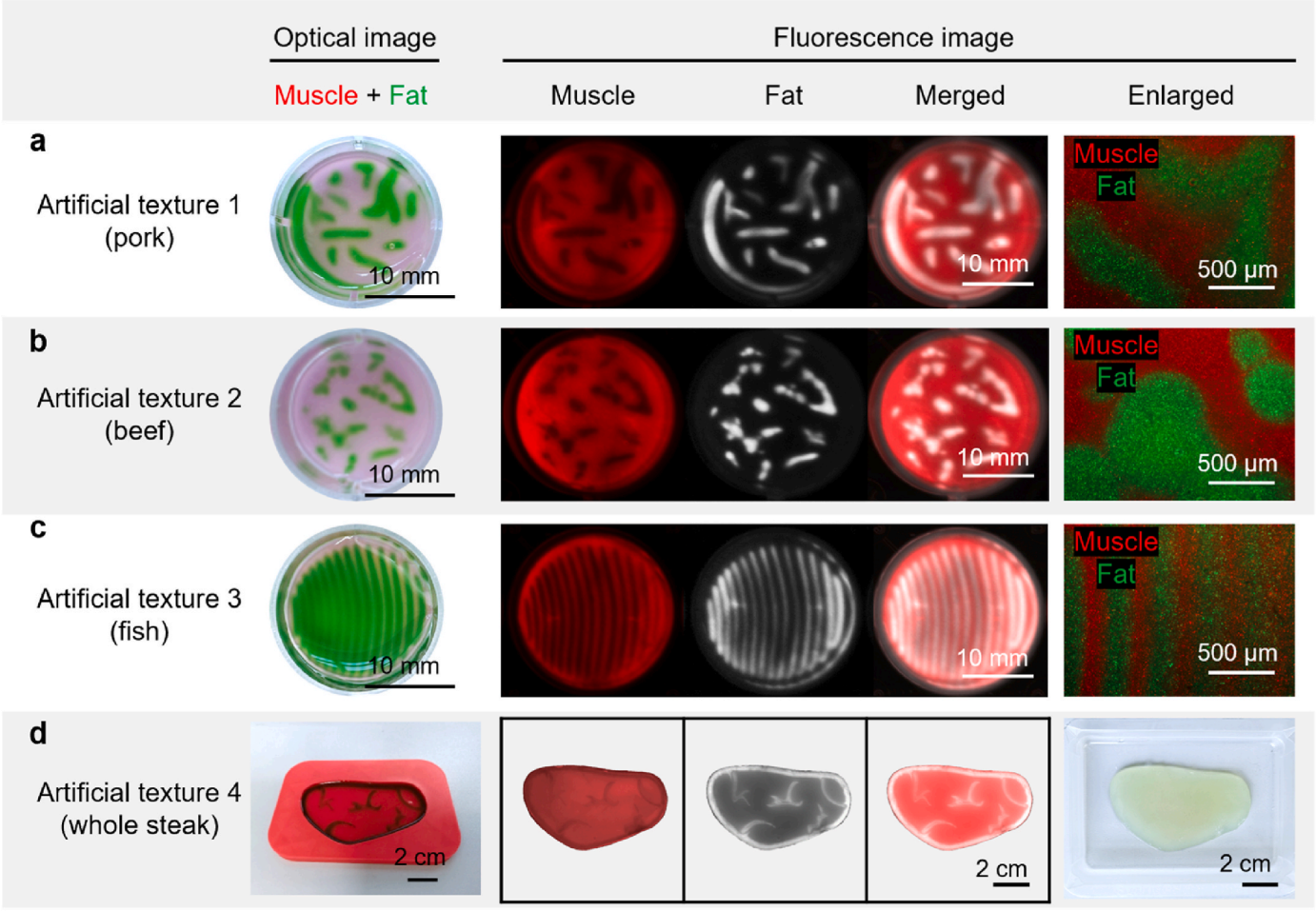

Fig. 4. Embedded bioprinting of artificial meat structures with various structures. Muscle bioink, composed of red dye and red fluorescent cells (HEK293-RFP), was cast into a 12-well plate or a steak mold, while the adipose component, containing green dye and green fluorescent cells (HEK293-GFP), was bioprinted within the muscle bioink. The resulting artificial meat constructs designed to replicate the structures of pork (a), beef (b), fish (c), and a whole steak (in a 3D printed plastic mold made from red PLA filament) (d), are shown as optical images (left panel), fluorescence images captured by the ChemiDoc Imaging System (middle panel), and fluorescence microscopy images (right panel). A crosslinked, bioprinted whole steak with thickness of around 1 cm is also displayed in the bottom right corner of the figure.

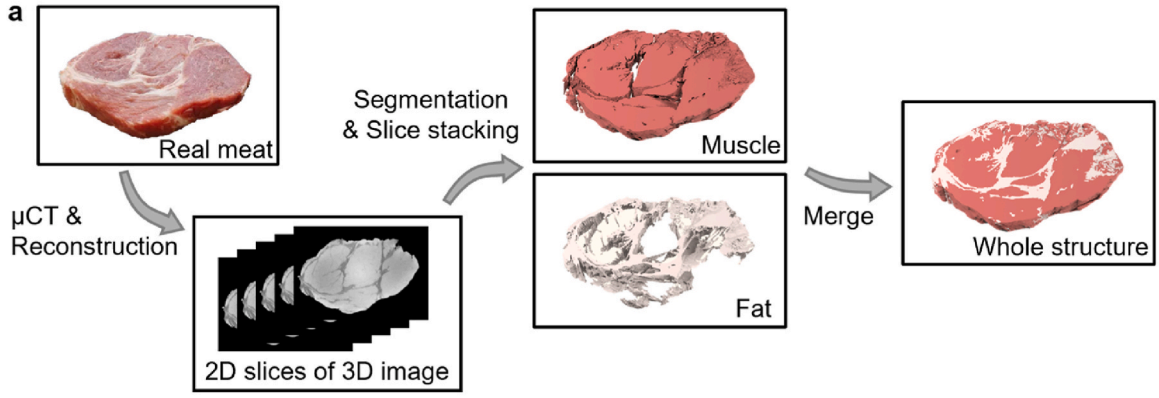

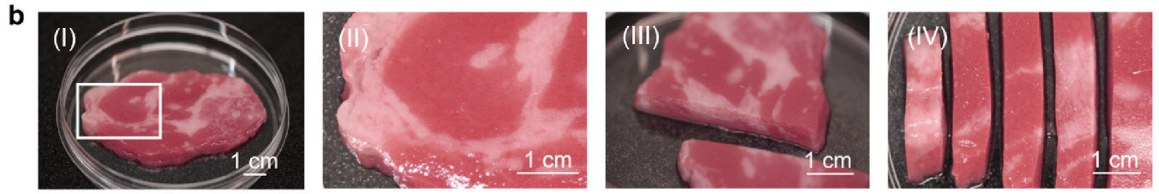

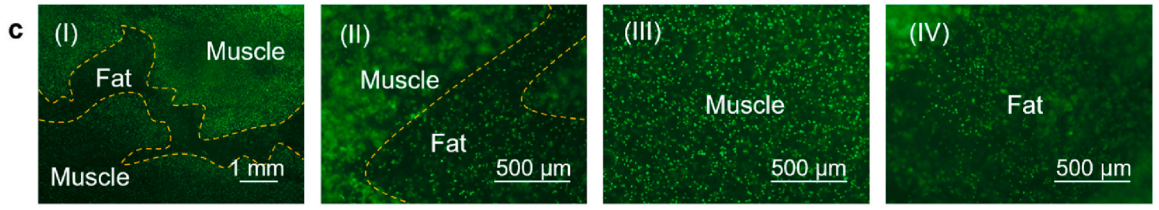

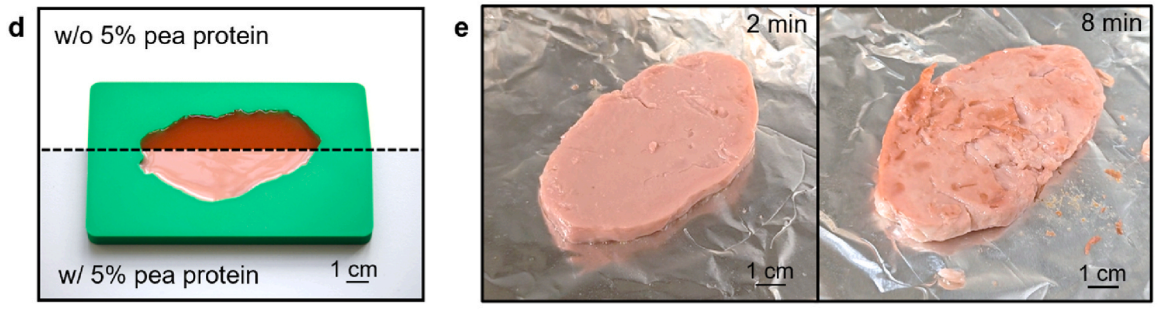

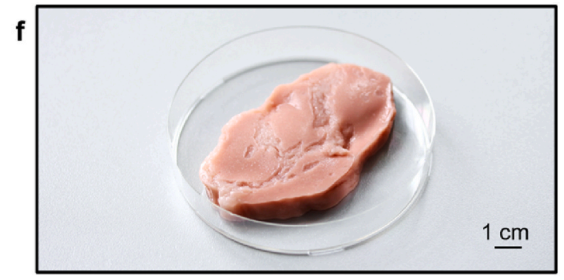

g

Component	Content /100g
Alginate	2.20 g
Pea protein	4.47 g
Porcine Fibroblasts	4.47 x 10^8 cells
Porcine adipocytes	1.04 x 10^8 cells

Fig. 5. Generation of a pork steak with natural meat structure. (a) Schematic representation of the process used to obtain natural pork structures, including both muscle and fat components, through μCT scanning and segmentation technology. (b) Images of the fabricated pork steak. An overview of the bioprinted pork steak in a Petri dish after crosslinking (I). An enlarged view of the pork steak showing detailed muscle and fat patterns (II). The bioprinted pork steak was sliced to show the cross-section (III). The pork steak was also cut into small pieces to highlight the spatial distribution of the fat component within the muscle (IV). (c) Fluorescence images of the bioprinted pork steak. After bioprinting, living cells were stained with Calcein AM (green signal) in the bioprinted and crosslinked pork steak, and observed under a fluorescence microscope. The yellow dashed lines indicate the borders between the muscle and fat regions (I and II). The distribution of both muscle and fat cells was well-preserved. (d) Optical images of the cast muscle component, where the upper half shows the original formulation, while the lower half includes an additional 5 % pea protein. (e) A piece of the cast muscle component was fried with olive oil on a digital hot plate. (f) Overview of the bioprinted pork steak incorporating 5 % pea protein in the muscle phase based on the original formulation. (g) Composition table of the bioprinted pork steak with pea protein, detailing the contents of alginate, pea protein, porcine fibroblasts, and adipocytes.

3.5. Fabrication and characterization of a meat product with natural structure

Based on the insights we gained from the previous experiments to fabricate customized meat-mimicking structures using embedded bioprinting, we advanced our research to replicate the intricate architecture of a natural meat product. Specifically, we focused on creating a pork steak model that accurately mirrors the native distribution of muscle and adipose tissues, utilizing advanced imaging and bioprinting techniques.

To faithfully replicate natural meat structures, we employed μCT imaging to capture high-resolution spatial information from an actual pork steak sample (Fig. 5a). The process began with μCT scanning to generate two-dimensional cross-sectional images, which were post-processed using ImageJ program and a self-developed Python script to remove artifacts, particularly high pixel noise and exposure attenuation along the inward axial direction (Supplementary Fig. 8). This refinement enabled precise differentiation between muscle and fat tissues based on subtle density variations. The processed images were then segmented and spatially stacked into separate 3D models of the muscle (major component) and fat (minor component), which were integrated to form a comprehensive digital representation of the pork steak's architecture. This approach allowed us to accurately replicate the complex marbling patterns that play a crucial role in the structure and sensory qualities of meat products.

Following digital modeling, we applied embedded bioprinting to fabricate a pork steak-like construct using the 2 % alginate hydrogel combined with porcine cells. To enhance visual realism, an oil-based food dye was mixed into the alginate bioink before printing, forming an oil-hydrogel emulsion. In this system, oil-based dye particles were dispersed and formed microparticles of the pigment, effectively encapsulated by the water-based alginate hydrogel. The dyes used in this study were tested and found not to interfere with fluorescence detection at the observed imaging depths (Supplementary Fig. 9). Optical imaging (Fig. 5b, I and II) confirmed that the bioprinted construct successfully reproduced the natural marbling and irregular fat distribution characteristic of real pork. The fat components were distinctly embedded within the muscle matrix, closely aligning with the spatial arrangement defined in the computational model (Fig. 5b, III and IV). Cross-sectional analyses further revealed that adipose regions were consistently distributed throughout the muscle tissue, underscoring the ability of embedded bioprinting to replicate complex internal structures that influence texture, flavor, and overall consumer appeal.

To assess cell viability and spatial precision within the bioprinted structure, fluorescence microscopy was performed (Fig. 5c). Calcein AM staining confirmed strong cell viability post-bioprinting, with intense green fluorescence observed in both muscle and adipose regions. High-magnification imaging revealed well-defined interfaces between the muscle and fat tissues, with cells uniformly distributed within their respective bioinks. These findings validate the cytocompatibility of the 2 % alginate hydrogel matrix and demonstrate that embedded bioprinting effectively preserves cellular organization in a spatial manner, a critical factor for achieving the desired sensory properties in cultured meat.

To enhance the nutritional profile of the bioprinted steak, 5 % pea protein was incorporated into the muscle phase. We then included cells and the fat component to the pea protein hydrogel. As shown in Fig. 5d, this addition resulted in a slight color fading, attributed to the naturally grayish hue of pea protein. To perform a practical test, we fried the cast muscle component with olive oil to evaluate its performance under real-life cooking conditions. As shown in Fig. 5e, the material maintained its structure over approximately 8 min of cooking and developed an appealing brown color. Using this modified muscle bioink, a structured pork steak-like construct was fabricated based on a μCT-derived model, exhibiting a well-defined architecture (Fig. 5f). The main constituents of the construct, including alginate, pea protein, porcine fibroblasts, and adipocytes, were analyzed and summarized in Fig. 5g.

The fat-phase formulation can similarly be tailored to achieve varying fat content and flavor profiles. This modularity allows precise customization of key sensory and nutritional attributes such as juiciness, flavor intensity, tenderness, and protein content—factors that are essential for consumer acceptance and commercial viability (Frank et al., 2016; Lambert et al., 2024).

4. Discussion

Embedded bioprinting offers a promising route to engineer complex food structures with precise spatial organization. Unlike traditional extrusion bioprinting, which struggles to maintain structural integrity in air, embedded approaches allow for fine-scale deposition within a stabilizing support bath (Bakirci et al., 2025; Y. Wu, Pang, et al., 2024). This advantage has been previously demonstrated in engineering vascularized 3D organ models (Cho et al., 2025; Fang et al., 2023; Zhang et al., 2023), but remains rarely explored for food-grade constructs. In this study, we applied embedded bioprinting to cultured meat fabrication, showing that it enabled faithful recreation of macroscale and microscale meat features, including species-specific muscle-fat arrangements such as beef marbling and fish layering.

A critical component in this process was the development of a suitable bioink system. While previous studies have employed collagen or gelatin-based inks (Ning et al., 2020; Reynolds et al., 2023), we identified 2 % alginate as an optimal formulation, balancing printability, biocompatibility, and post-crosslinking mechanical stability. Interestingly, porcine adipocytes not only survived within the alginate matrix but also demonstrated robust lipid accumulation, suggesting the matrix allows sufficient exchange of adipogenic cues. This performance is comparable to previous reports using fibrinogen/alginate (Guan et al., 2025) or gelatin methacryloyl (Jeong et al., 2022), but with the added advantage of animal-free origin and lower cost. Nonetheless, alginate lacks intrinsic bioactivity, and future improvements may require functionalization or blending with protein-based components to support better cell behaviors, such as cell adhesion, spreading and self-organization.

To further enhance the realism of bioprinted meat, we integrated μCT imaging with computational modeling to replicate the native architecture of pork steak. While μCT has been widely used in biomedical imaging, its application in cultured meat design remains largely unexplored. Previous approaches to structuring cultured meat have relied primarily on models from computer-aided design or visual estimations of muscle-fat patterns (Dutta et al., 2022; Kang et al., 2021; Park et al., 2023; Schüler et al., 2024). In contrast, our pipeline captures authentic tissue architecture from natural meat cuts, which may better support consumer perception and product authenticity.

However, this approach presents challenges. Soft tissue μCT imaging is limited by low contrast between muscle and fat, and signal attenuation in deeper regions can compromise resolution and hinder precise segmentation (Ay & Zaidi, 2006; Wang et al., 2021). These issues were addressed by employing a custom Python-based correction algorithm. It enabled accurate segmentation of different tissue structures by exposure correction pixel-wisely. Yet, finer structures such as connective tissue, vasculature, or intramuscular fiber orientation remain difficult to resolve. Future integration with multimodal imaging—such as MRI or optical coherence tomography—may provide higher fidelity templates for next-generation meat constructs.

Despite these advancements, several challenges remain in scaling this technology from laboratory research to commercial production. While the 2 % alginate hydrogel demonstrated favorable rheological and cellular properties in the short term, challenges persist regarding long-term cell proliferation, maturation, and differentiation within the matrix. Furthermore, in addition to pea protein, other plant-based proteins, as well as methyl cellulose and starch, can also be incorporated to enhance the overall nutritional value and broaden the range of suitable

cooking methods (Sá, Franco, & and Carciofi, 2020; Vu et al., 2022). Additionally, the development of animal-free culture media is essential to achieving ethical and cost-effective large-scale production. Current formulations often rely on animal-derived components, such as fetal bovine serum (FBS) (D. Y. Lee et al., 2022), which contradict the ethical goals of cultured meat. Future research should focus on optimizing hydrogel formulations, microstructure formation, engineering cell lines, and developing bioactive culture environments to promote muscle fiber formation and adipose tissue maturation.

Scalability remains another key challenge for commercialization (Soleymani et al., 2024). The bioprinting process must balance speed, structural resolution, and cellular viability. Implementing parallel processing with multiple extrusion nozzles for fat and muscle components could significantly enhance production efficiency. Moreover, printing larger meat constructs introduces challenges during culture and maturation, chiefly limited nutrient diffusion and the development of hypoxic conditions in deeper layers. The integration of vascular-like networks or perfusion systems could address these issues by ensuring adequate oxygen and nutrient delivery to all cells within the printed structure (Kolesky et al., 2016; D. Wu, Pang, et al., 2024).

Beyond structural accuracy, achieving desirable sensory attributes, such as texture, flavor, aroma, and mouthfeel, will be crucial for consumer acceptance. Future studies should incorporate comprehensive texture analysis and sensory evaluations with trained panels and consumer testing to ensure that bioprinted cultured meat meets industry standards and market expectations.

5. Conclusion

This study demonstrates that embedded bioprinting, combined with optimized alginate hydrogel bioinks, μCT-based modeling, and advanced fabrication techniques, enables the reproducible production of realistic, structurally accurate cultured meat products. This approach provides exceptional flexibility for replicating natural meat architectures, establishing embedded bioprinting as a promising tool for sustainable, customizable, and scalable meat production. However, to transition from laboratory-scale research to practical food applications, further improvements are required in bioink formulations, long-term cellular functionality, sensory optimization, and production scalability. Continued advancements in these areas will move embedded bioprinting closer to commercial viability, supporting the development of sustainable, high-quality cultured meat that aligns with global food security, environmental sustainability, and ethical considerations.

CRediT authorship contribution statement

Dongwei Wu: Writing – review & editing, Writing – original draft, Visualization, Validation, Methodology, Investigation, Formal analysis, Conceptualization. **Shumin Pang:** Writing – review & editing, Validation, Investigation. **Sabrina Bäther:** Writing – review & editing, Investigation. **Lisa Woelken:** Writing – review & editing, Investigation. **Mariia Abyzova:** Writing – review & editing, Investigation. **Jordi Morales-Dalmau:** Writing – review & editing, Resources. **Astrid Haibel:** Writing – review & editing, Resources, Investigation. **Yunpeng Jia:** Writing – review & editing, Software, Investigation. **Johanna Berg:** Writing – review & editing, Investigation. **Benedikt B. Kaufer:** Writing – review & editing, Resources. **Caroline Denesvre:** Writing – review & editing, Resources. **Anja Maria Wagemans:** Writing – review & editing, Resources, Funding acquisition. **Cornelia Rauh:** Writing – review & editing, Resources, Funding acquisition. **Jens Kurreck:** Writing – review & editing, Writing – original draft, Supervision, Resources, Funding acquisition, Conceptualization.

Declaration of generative AI and AI-assisted technologies in the writing process

During the preparation of this work the authors used ChatGPT in order to improve language and readability. After using this tool, the authors reviewed and edited the content as needed and take full responsibility for the content of the publication.

Declaration of competing interest

The authors declare the following financial interests/personal relationships which may be considered as potential competing interests: Mariia Abyzova and Jordi Morales-Dalmau are employees of Cultimate Foods GmbH (Berlin/Hannover). However, the authors declare that they contributed to this study objectively and without bias. The company did not influence manuscript preparation. No other conflicts of interest exist. All other authors declare that they have no known competing financial interests or personal relationships that could have appeared to influence the work reported in this paper.

Acknowledgements

This IGF Project of the FEI was supported within the program for promoting the Industrial Collective Research ("Industrielle Gemeinschaftsforschung", IGF) of the German Ministry of Economics and Climate Action (BMWK), based on a resolution of the German Parliament. Project 01IF22232N.

Appendix A. Supplementary data

Supplementary data to this article can be found online at https://doi.org/10.1016/j.foodhyd.2025.111795.

Data availability

Data will be made available on request.

References

Albrecht, F. B., Ahlfeld, T., Klatt, A., Heine, S., Gelinsky, M., & Kluger, P. J. (2024). Biofabrication's contribution to the evolution of cultured meat. *Advanced Healthcare Materials, 13*(13), Article 2304058.

Ay, M. R., & Zaidi, H. (2006). Assessment of errors caused by X-ray scatter and use of contrast medium when using CT-based attenuation correction in PET. *European Journal of Nuclear Medicine and Molecular Imaging, 33*(11), 1301–1313.

Aydemir, D., Sarayloo, E., & Nuray, U. N. (2020). Rosiglitazone-induced changes in the oxidative stress metabolism and fatty acid composition in relation with trace element status in the primary adipocytes. *Journal of Medical Biochemistry, 39*(3), 267.

Bakirci, E., Asghari Adib, A., Ashraf, S. F., & Feinberg, A. W. (2025). Advancing extrusion-based embedded 3D bioprinting via scientific, engineering, and process innovations. *Biofabrication, 17*(2), Article 023002.

Bäther, S., Seibt, J. H., Hundschell, C. S., Bonilla, J. C., Clausen, M. P., & Wagemans, A. M. (2024). Phase behaviour and structure formation of alginate-gelatin composite gels. *Food Hydrocolloids, 149*, Article 109538.

Berg, J., & Kurreck, J. (2021). Clean bioprinting - Fabrication of 3D organ models devoid of animal components. *ALTEX - Alternatives to Animal Experimentation, 38*(2), 269–288.

Cho, W.-W., Park, W., & Cho, D.-W. (2025). Recent trends in embedded 3D bioprinting of vascularized tissue constructs. *Biofabrication, 17*(2), Article 022002.

Choi, I., Lee, Y., Lyu, J. S., Lee, J.-S., & Han, J. (2022). Characterization of ionically crosslinked alginate films: Effect of different anion-based metal cations on the improvement of water-resistant properties. *Food Hydrocolloids, 131*, Article 107785.

Contador, D., Ezquer, F., Espinosa, M., Arango-Rodriguez, M., Puebla, C., Sobrevia, L., & Conget, P. (2015). Featured article: Dexamethasone and rosiglitazone are sufficient and necessary for producing functional adipocytes from mesenchymal stem cells. *Experimental Biology and Medicine, 240*(9), 1235–1246.

Dimitriadis, G., Mitrou, P., Lambadiari, V., Maratou, E., & Raptis, S. A. (2011). Insulin effects in muscle and adipose tissue. *Diabetes Research and Clinical Practice, 93*, S52–S59.

Dutta, S. D., Ganguly, K., Jeong, M.-S., Patel, D. K., Patil, T. V., Cho, S.-J., & Lim, K.-T. (2022). Bioengineered lab-grown meat-like constructs through 3D bioprinting of antioxidative protein hydrolysates. *ACS Applied Materials & Interfaces, 14*(30), 34513–34526.

Fang, Y., Guo, Y., Wu, B., Liu, Z., Ye, M., Xu, Y., Ji, M., Chen, L., Lu, B., Nie, K., Wang, Z., Luo, J., Zhang, T., Sun, W., & Xiong, Z. (2023). Expanding embedded 3D bioprinting capability for engineering complex organs with freeform vascular networks. *Advanced Materials, 35*(22), Article 2205082.

Frank, D., Joo, S.-T., & Warner, R. (2016). Consumer acceptability of intramuscular fat. 한국축산식품학회지, *36*(6), 699–708.

Godde, C. M., Mason-D'Croz, D., Mayberry, D. E., Thornton, P. K., & Herrero, M. (2021). Impacts of climate change on the livestock food supply chain; a review of the evidence. *Global Food Security, 28*, Article 100488.

Guan, X., Fei, Z., Wang, L., Ji, G., Du, G., Ma, Z., & Zhou, J. (2025). Engineered streaky pork by 3D co-printing and co-differentiation of muscle and fat cells. *Food Hydrocolloids, 158*, Article 110578.

Guo, X., Wang, D., He, B., Hu, L., & Jiang, G. (2024). 3D bioprinting of cultured meat: A promising avenue of meat production. *Food and Bioprocess Technology, 17*(7), 1659–1680.

Gurel, M., Rathod, N., Cabrera, L. Y., Voyton, S., Yeo, M., Ozogul, F., & Ozbolat, I. T. (2024). A narrative review: 3D bioprinting of cultured muscle meat and seafood products and its potential for the food industry. *Trends in Food Science & Technology, 152*, Article 104670.

Handral, K., Shi, H. T., Weng, W. C., & Choudhury, D. (2022). 3D printing of cultured meat products. *Critical Reviews in Food Science and Nutrition, 62*(1), 272–281.

Jeong, D., Seo, J. W., Lee, H.-G., Jung, W. K., Park, Y. H., & Bae, H. (2022). Efficient myogenic/adipogenic transdifferentiation of bovine fibroblasts in a 3D bioprinting system for steak-type cultured meat production. *Advanced Science, 9*(31), Article 2202877.

Kang, D.-H., Louis, F., Liu, H., Shimoda, H., Nishiyama, Y., Nozawa, H., Kakitani, M., Takagi, D., Kasa, D., Nagamori, E., Irie, S., Kitano, S., & Matsusaki, M. (2021). Engineered whole cut meat-like tissue by the assembly of cell fibers using tendon-gel integrated bioprinting. *Nature Communications, 12*(1), 5059.

Klatt, A., Wollschlaeger, J. O., Albrecht, F. B., Rühle, S., Holzwarth, L. B., Hrenn, H., Melzer, T., Heine, S., & Kluger, P. J. (2024). Dynamically cultured, differentiated bovine adipose-derived stem cell spheroids as building blocks for biofabricating cultured fat. *Nature Communications, 15*(1), 9107.

Kolesky, D. B., Homan, K. A., Skylar-Scott, M. A., & Lewis, J. A. (2016). Three-dimensional bioprinting of thick vascularized tissues. *Proceedings of the National Academy of Sciences, 113*(12), 3179–3184.

Lambert, E. G., O'Keeffe, C. J., Ward, A. O., Anderson, T. A., Yip, Q., & Newman, P. L. H. (2024). Enhancing the palatability of cultivated meat. *Trends in Biotechnology, 42*(9), 1112–1127.

Lee, M., Choi, W., Lee, J. M., Lee, S. T., Koh, W.-G., & Hong, J. (2024). Flavor-switchable scaffold for cultured meat with enhanced aromatic properties. *Nature Communications, 15*(1), 5450.

Lee, D. Y., Lee, S. Y., Yun, S. H., Jeong, J. W., Kim, J. H., Kim, H. W., Choi, J. S., Kim, G.-D., Joo, S. T., Choi, I., & Hur, S. J. (2022). Review of the current research on fetal bovine serum and the development of cultured meat. *Food Science of Animal Resources, 42*(5), 775–799.

Liu, L. F., Purushotham, A., Wendel, A., Koba, K., DeIuliis, J., Lee, K., & Belury, M. A. (2009). Regulation of adipose triglyceride lipase by rosiglitazone. *Diabetes, Obesity and Metabolism, 11*(2), 131–142.

Marques, D. M. C., Jabouille, M., Gusmão, A., Leite, M., Sanjuan-Alberte, P., & Ferreira, F. C. (2025). Microalgae-enriched (bio)inks for 3D bioprinting of cultured seafood. *Npj Science of Food, 9*(1), 23.

Martins, B., Bister, A., Dohmen, R. G. J., Gouveia, M. A., Hueber, R., Melzener, L., Messmer, T., Papadopoulos, J., Pimenta, J., Raina, D., Schaeken, L., Shirley, S., Bouchet, B. P., & Flack, J. E. (2024). Advances and challenges in cell biology for cultured meat. *Annual Review of Animal Biosciences, 12*(2024), 345–368.

Meyers, W. H., & Kalaitzandonakes, N. (2015). World population, food growth, and food security challenges. *Food Security in an Uncertain World, 15*, 161–177. Emerald Group Publishing Limited.

Mills, S. E. (1999). Regulation of porcine adipocyte metabolism by insulin and adenosine. *Journal of Animal Science, 77*(12), 3201–3207.

Ning, L., Mehta, R., Cao, C., Theus, A., Tomov, M., Zhu, N., Weeks, E. R., Bauser-Heaton, H., & Serpooshan, V. (2020). Embedded 3D bioprinting of gelatin methacryloyl-based constructs with highly tunable structural fidelity. *ACS Applied Materials & Interfaces, 12*(40), 44563–44577.

Ozbolat, I. T., Peng, W., & Ozbolat, V. (2016). Application areas of 3D bioprinting. *Drug Discovery Today, 21*(8), 1257–1271.

Park, S., Hong, Y., Park, S., Kim, W., Gwon, Y., Jang, K.-J., & Kim, J. (2023). Designing highly aligned cultured meat with nanopatterns-assisted bio-printed fat scaffolds. *Journal of Biosystems Engineering, 48*(4), 503–511.

Post, M. J., Levenberg, S., Kaplan, D. L., Genovese, N., Fu, J., Bryant, C. J., Negowetti, N., Verzijden, K., & Moutsatsou, P. (2020). Scientific, sustainability and regulatory challenges of cultured meat. *Nature Food, 1*(7), 403–415.

Reynolds, D. S., de Lázaro, I., Blache, M. L., Liu, Y., Jeffreys, N. C., Doolittle, R. M., Grandidier, E., Olszewski, J., Dacus, M. T., Mooney, D. J., & Lewis, J. A. (2023). Microporogen-structured collagen matrices for embedded bioprinting of tumor models for immuno-oncology. *Advanced Materials, 35*(33), Article 2210748.

Roy, B. C., & Bruce, H. L. (2024). Contribution of intramuscular connective tissue and its structural components on meat tenderness-revisited: A review. *Critical Reviews in Food Science and Nutrition, 64*(25), 9280–9310.

Sá, A. G. A., Franco, M. Y. M., & Carciofi, B. A. M. (2020). Food processing for the improvement of plant proteins digestibility. *Critical Reviews in Food Science and Nutrition, 60*(20), 3367–3386.

Santoni, S., Gugliandolo, S. G., Sponchioni, M., Moscatelli, D., & Colosimo, B. M. (2022). 3D bioprinting: Current status and Trends—A guide to the literature and industrial practice. *Bio-Design and Manufacturing, 5*(1), 14–42.

Schätzlein, E., & Blaeser, A. (2022). Recent trends in bioartificial muscle engineering and their applications in cultured meat, biorobotic systems and biohybrid implants. *Communications Biology, 5*(1), 737.

Schüler, K., Marques, D. M. C., Gusmão, A., Jabouille, M., Leite, M., Cabral, J. M. S., Sanjuan-Alberte, P., & Ferreira, F. C. (2024). 3D printing of plant-based fat inks towards manufacturing complex cellular agriculture products with fatty structures. *Food Hydrocolloids, 157*, Article 110369.

Soleymani, S., Naghib, S. M., & Mozafari, M. R. (2024). An overview of cultured meat and stem cell bioprinting: How to make it, challenges and prospects, environmental effects, society's culture and the influence of religions. *Journal of Agriculture and Food Research, 18*, Article 101307.

Tao, L., Shi, C., Zi, Y., Zhang, H., Wang, X., & Zhong, J. (2024). A review on the chemical modification of alginates for food research: Chemical nature, modification methods, product types, and application. *Food Hydrocolloids, 147*, Article 109338.

Vautherot, J.-F., Jean, C., Fragnet-Trapp, L., Rémy, S., Chabanne-Vautherot, D., Montillet, G., Fuet, A., Denesvre, C., & Pain, B. (2017). ESCDL-1, a new cell line derived from chicken embryonic stem cells, supports efficient replication of mardiviruses. *PLoS One, 12*(4), Article e0175259.

Vu, G., Zhou, H., & McClements, D. J. (2022). Impact of cooking method on properties of beef and plant-based burgers: Appearance, texture, thermal properties, and shrinkage. *Journal of Agriculture and Food Research, 9*, Article 100355.

Wanapat, M., Suriyapha, C., Dagaew, G., Matra, M., Phupaboon, S., Sommai, S., Pongsub, S., & Muslykhah, U. (2024). Sustainable livestock production systems are key to ensuring food security resilience in response to climate change. *Agriculture and Natural Resources, 58*(4), 537–546.

Wang, X., Wang, G., Xiao, Y., Zuo, Y., & Zhou, F. (2021). A nondestructive method of measuring zebrafish adipose tissue based on micro-computed tomography (Micro-CT). *Applied Sciences, 11*(22), Article 10510.

Williams, K. J., Picou, A. A., Kish, S. L., Giraldo, A. M., Godke, R. A., & Bondioli, K. R. (2008). Isolation and characterization of porcine adipose tissue-derived adult stem cells. *Cells Tissues Organs, 188*(3), 251–258.

Woelken, L., Weckowska, D. M., Dreher, C., & Rauh, C. (2024). Toward an innovation radar for cultivated meat: Exploring process technologies for cultivated meat and claims about their social impacts. *Frontiers in Sustainable Food Systems, 8*.

Wu, D., Berg, J., Arlt, B., Röhrs, V., Al-Zeer, M. A., Deubzer, H. E., & Kurreck, J. (2022). Bioprinted cancer model of neuroblastoma in a renal microenvironment as an efficiently applicable drug testing platform. *International Journal of Molecular Sciences, 23*(1), 122.

Wu, D., Pang, S., Berg, J., Mei, Y., Ali, A. S. M., Röhrs, V., Tolksdorf, B., Hagenbuchner, J., Ausserlechner, M. J., Deubzer, H. E., Gurlo, A., & Kurreck, J. (2024). Bioprinting of perfusable vascularized organ models for drug development via sacrificial-free direct ink writing. *Advanced Functional Materials, 34*(30), Article 2314171.

Wu, Y., Yang, X., Gupta, D., Alioglu, M. A., Qin, M., Ozbolat, V., Li, Y., & Ozbolat, I. T. (2024). Dissecting the interplay mechanism among process parameters toward the biofabrication of high-quality shapes in embedded bioprinting. *Advanced Functional Materials, 34*(21), Article 2313088.

Zeng, X., Meng, Z., He, J., Mao, M., Li, X., Chen, P., Fan, J., & Li, D. (2022). Embedded bioprinting for designer 3D tissue constructs with complex structural organization. *Acta Biomaterialia, 140*, 1–22.

Zhang, S., Qi, C., Zhang, W., Zhou, H., Wu, N., Yang, M., Meng, S., Liu, Z., & Kong, T. (2023). In situ endothelialization of free-form 3D network of interconnected tubular channels via interfacial coacervation by aqueous-in-aqueous embedded bioprinting. *Advanced Materials, 35*(7), Article 2209263.

Update

Food Hydrocolloids

Volume 173, Issue , April 2026, Page

DOI: https://doi.org/10.1016/j.foodhyd.2025.112251

Food Hydrocolloids 173 (2026) 112251

Contents lists available at ScienceDirect

Food Hydrocolloids

journal homepage: www.elsevier.com/locate/foodhyd

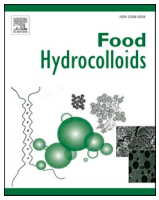

Corrigendum to "Embedded bioprinting enables precise fabrication of cultured meat with authentic structural properties" [Food Hydrocolloids 171 (2026) 111795]

Dongwei Wu [a], Shumin Pang [a,b], Sabrina Bäther [c,d], Lisa Woelken [e], Mariia Abyzova [f,g], Jordi Morales-Dalmau [g], Astrid Haibel [h], Yunpeng Jia [i], Johanna Berg [a], Benedikt B. Kaufer [j], Caroline Denesvre [k], Anja Maria Wagemans [c,d], Cornelia Rauh [e], Jens Kurreck [a,*]

[a] Technische Universität Berlin, Chair of Applied Biochemistry, Straße des 17. Juni 135, 10623, Berlin, Germany
[b] Technische Universität Berlin, Chair of Advanced Ceramic Materials, Straße des 17. Juni 135, 10623, Berlin, Germany
[c] Technische Universität Berlin, Department of Food Biosciences, Straße des 17. Juni 135, 10623, Berlin, Germany
[d] Technische Universität Dresden, Chair of Food Engineering, Bergstraße 120, 01069, Dresden, Germany
[e] Technische Universität Berlin, Department of Food Biotechnology and Food Process Engineering, Straße des 17. Juni 135, 10623, Berlin, Germany
[f] Leibniz University of Hanover, Institute of Technical Chemistry, Hanover, Germany
[g] Cultimate Foods GmbH, Berlin/Hannover, Germany
[h] Berliner Hochschule für Technik, Fachbereich II Mathematics-Physics-Chemistry, Luxemburger Str. 10, 13353, Berlin, Germany
[i] Birmingham City University, Department of Life Science, Faculty of Health, Education and Life Sciences, Birmingham, UK
[j] Freie Universität Berlin, Institute of Virology, Berlin, Germany
[k] INRAE, Université de Tours, ISP, Equipe Biologie des Virus Aviaires, F-37380, Nouzilly, France

Only after publication of the study did we learn, through mitochondrial sequencing, that the fibroblasts we received were of murine rather than the presumed porcine origin. These cells were used in the experiments shown in Figs. 2C and 5. While the use of murine cells would not be appropriate for a final cultured-meat product, this does not affect the conclusions of our study. Our aim was to demonstrate that fibroblasts and adipocytes can be organized into two distinct structures to mimic the natural architecture of steak using bioprinting. This concept and the scientific findings remain valid regardless of the species origin of the cells.

We regret this error and thank Dr. Jörg Plötner and Robert Schreiber for the molecular identification of the species. We also appreciate the efforts of the group that supplied the cells and emphasize that this was an honest and unintended oversight.

DOI of original article: https://doi.org/10.1016/j.foodhyd.2025.111795.
* Corresponding author.
E-mail address: Jens.kurreck@tu-berlin.de (J. Kurreck).

https://doi.org/10.1016/j.foodhyd.2025.112251

Available online 15 November 2025